2019-12-27

An Evaluation of Kolmogorov's 5/3 Power Law Observed Within the Turbulent Airflow Above the Ocean

OrtizSuslow, David G.; Wang, Qing

AGU

OrtizSuslow, D. G., & Wang, Q. (2019). An evaluation of Kolmogorov's 5/3 power law observed within the turbulent airflow above the ocean. Geophysical Research Letters, 46, 14,90114,911.

http://hdl.handle.net/10945/66915

AGU100 ADVANCING EARTH AND SPACE SCIENCE

Geophysical Research Letters

RESEARCH LETTER
10.1029/2019GL085083

An Evaluation of Kolmogorov's −5/3 Power Law Observed Within the Turbulent Airflow Above the Ocean

David G. Ortiz-Suslow[1] and Qing Wang[1]

[1]Department of Meteorology, Naval Postgraduate School, Monterey, CA, USA

Key Points:
- A new empirical method is used to conduct the first observational investigation of Kolmogorov's −5/3 law in the airflow above the ocean
- While −5/3 was generally valid, deviations were strongly linked to surface layer dynamics and air-sea interaction
- The observed inertial subrange power varied with altitude, wind speed, wave age, and atmospheric stability

Supporting Information:
- Supporting Information S1

Correspondence to:
D. G. Ortiz-Suslow, and Q. Wang,
dortizsu@nps.edu
qwang@nps.edu

Citation:
Ortiz-Suslow, D. G., & Wang, Q. (2019). An evaluation of Kolmogorov's −5/3 power law observed within the turbulent airflow above the ocean. *Geophysical Research Letters*, *46*, 14,901–14,911. https://doi.org/10.1029/2019GL085083

Received 21 AUG 2019
Accepted 9 DEC 2019
Accepted article online 13 DEC 2019
Published online 27 DEC 2019

The copyright line for this article was changed on 26 NOV 2020 after original online publication.

Abstract In 1941, Kolmogorov postulated that the energy distribution of turbulence, across a particular range of eddy sizes cascading to dissipation, could be uniquely described as a universal −5/3 power law. This theory was readily accepted as the basis for conceptualizing the phenomenological characteristics of turbulence and remains central to continued experimental and theoretical developments in turbulence study. However, the theory's own validity lacks final certainty. Here we present the first observation-based evaluation of Kolmogorov's power law within the atmospheric flow above the ocean. Using a unique platform and a novel analytical approach, we found that the expected power law varies systematically with height above the surface and the local environmental state. Our findings suggest that Kolmogorov's idealized value (−5/3) is approximately valid but, under certain conditions, may depend strongly on the unique processes and dynamics near the ocean surface. This discovery should motivate a reevaluation of how Kolmogorov's framework is applied to geophysical turbulence in the vicinity of the air-sea interface.

Plain Language Summary In 1941, a Russian scientist (A. N. Kolmogorov) put forth a relatively straight-forward solution to the question that had puzzled fluid scientists and keen observers for a long time: how the large scale fluid motions, which have kinetic energy (E), engender the fine-scale whorls and eddies endemic in almost any sufficiently vigorous fluid? In a nutshell, Kolmogorov's hypotheses to explain this stated that the distribution of E within the fluid follows a fairly simple formula with the universal power −5/3. Since it was proposed, this theory has formed the basis by which we conceptualize and study fluid turbulence. In the atmosphere, this −5/3 power law is used to study the fundamental physics underlying some of our most pressing problems: forecasting storm intensity, climate-regulating atmosphere-ocean exchange, and ocean wave growth. Using a unique ocean observing platform and a novel analytical method, we have conducted the first evaluation of Kolmogorov's −5/3 power law within the marine atmosphere. We demonstrate that this classical theory breaks down near the ocean surface, suggesting that ocean waves play a critical role in the atmospheric motion and energy balance. These findings provide tangible evidence that Kolmogorov's theory needs to be re-evaluated in the context of flow near ocean waves. While our work represents a unique and meaningful step to enhance our knowledge of turbulence theories, additional work is needed to fully understand the underlying physics.

1. Introduction

The eddies and whorls within a fluid flow have long captured the attention of perceptive observers, as being simultaneously coherent and unpredictable. Collectively, this motion is referred to as turbulence, which actively mixes energy and mass throughout a fluid volume, and is critical for a diversity of applications (Abraham, 1998; Martínez-Prat et al., 2019; Peinke et al., 2004; Wensink et al., 2012). The present basis for our theoretical understanding of turbulence came in 1941, when Kolmogorov proposed (Kolmogorov, 1941a, 1941ab) that the turbulence kinetic energy within a fluid exists across a spectrum of wave number (k), with known distribution $E = f(k, \epsilon, \nu)$, where ϵ is the ensemble mean dissipation rate and ν is the fluid viscosity. Under certain conditions, a subrange of the total energy spectrum will be independent of ν (Batchelor, 1947, 1953; Tennekes & Lumley, 1972),

$$E(k) = \alpha \epsilon^{2/3} k^{-5/3}, \tag{1}$$

where α is a constant ~1.5 (Hogstrom, 1996; Yaglom, 1981; Yeung & Zhou, 1997). Equation (1) is only valid over a wave number range, Δk, known as the inertial subrange. It became apparent later that Kolmogorov's concept of the ensemble average was idealized (Wyngaard, 2010) and a Reynolds number (Re) dependent relationship was proposed (Kolmogorov, 1962; Oboukhov, 1962), effectively causing $-5/3 \rightarrow -(5/3+\mu)$, where $\mu \sim \alpha_p / \ln(Re)$ (α_p is ~1). This adjustment describes intermittency's impact on ϵ, which increases in

low *Re* and high stratification (Barenblatt et al., 1997). Debate persists (Moffatt, 2002) on the impact and significance of μ in the practical application of (1) in the regime of high *Re* and low stratification (Barenblatt et al., 1997; Barenblatt & Chorin, 1997)—especially if only considering the second-order statistics (Arenas & Chorin, 2006). Furthermore, no analytical basis exists for systematically identifying Δk, i.e., the *actual* extent of the inertial subrange in Fourier space.

The atmosphere and ocean comprise a dynamic, visually stimulating, and inexorably coupled system whose physical linkage is maintained by turbulence generated via wind shear and heat flux across the interface between the marine atmospheric surface layer (MASL) and the upper ocean. Understanding and predicting this dynamic interaction is integral to addressing some of our most pressing problems: quantifying global air-sea gas exchange, forecasting tropical storm intensity, or maritime communication and national security. Our ability to tackle these problems and study these phenomena hinges on a fundamental understanding of the complex physics at the atmosphere-ocean interface. In the geophysical domain, and especially within the MASL, Kolmogorov's spectrum (1) is considered widely valid based on early field observations (MacCready, 1962; Payne & Lumley, 1966) and has been applied to quantify the energy dissipation and interfacial fluxes of momentum and heat (Edson et al., 1991; Large & Pond, 1981, 1982), as well as quantify other near-surface processes (Friehe et al., 1975; Lawrence et al., 1970). However, from a representative literature review, including some of the most regarded studies (Google: 7,500+ citations), we found no consistent method for applying (1) to obtain relevant parameters, such as the turbulence dissipation rate or the structure function parameters (Anderson, 1993; Drennan et al., 1999; Durand et al., 1991; Edson et al., 1991; Edson & Fairall, 1998; Fairall & Larsen, 1986; Grachev et al., 2018; Hackerott et al., 2017; Large & Pond, 1981, 1982; Muñoz-Esparza et al., 2018; Sjöblom & Smedman, 2002; Yelland & Taylor, 1996). Only a minority of studies directly stated how Δk was determined, some of whom imposed arbitrary limits (e.g., Yelland & Taylor, 1996). Many investigators solely relied on visual inspection, which is not unique to atmospheric studies (Barenghi et al., 2016). Furthermore, all of the previous works we reviewed assumed the theoretical $k^{-5/3}$ without confirming its validity; non-Kolmogorov measurements have been sparsely reported within the MASL (Dreyer, 1974; Friehe et al., 1975; Phelps & Pond, 1971) but were not fully explored.

Here we present the first observation-based evaluation of (1) within the MASL. We employ a novel technique (Ortiz-Suslow, Kalogiros, et al., 2019) that identifies the most probable Δk in a measured turbulence spectrum and empirically determines the power law over the inertial subrange. Our findings suggest that there are systematic deviations from Kolmogorov's $-5/3$, which may be driven by processes unique to the air-sea interface.

2. Turbulence Measurement and Analysis

2.1. Observations Made From *FLIP*

Turbulence measurements were made offshore of Southern California from the Floating Instrument Platform (*FLIP*, see Figure 1) during the Coupled Air-Sea Processes and Electromagnetic ducting Research (CASPER) field campaign (Wang et al., 2018). The observations were made with a vertical stack of three-dimensional

ultrasonic anemometers at 3–16 m above the ocean (see Figure 1). Due to its unique design (Fisher & Spiess, 1963), the over 65 year old *FLIP* remains the ideal platform making uncontaminated near-surface turbulence measurements (Grare et al., 2013; Miller et al., 2008). To date, our observations represent one of the most complete micrometeorological data sets for MASL study. The data processing was carried out following standard methods for data quality control, platform motion correction, and the eddy covariance technique for turbulence statistics. The impact of *FLIP*'s superstructure on the MASL flow and its potential impact on data quality was determined, and a wind sector was identified where platform's superstructure and mast apparatus significantly impacted the turbulence statistics. Samples where the mean azimuthal wind vector lay within this sector were not considered here. Further information regarding the data processing can be found in supporting information (S1) and a technical report (Ortiz-Suslow, Kalogiros, et al., 2019).

2.2. Locating Kolmogorov's Subrange

Kolmogorov's spectrum is fundamentally based on two conditions (Yeung & Zhou, 1997): (1) the kinetic energy (E) over Δk exhibits local isotropy and (2) that $E \propto k^{-5/3}$ across Δk. Isotropy is the concept that the

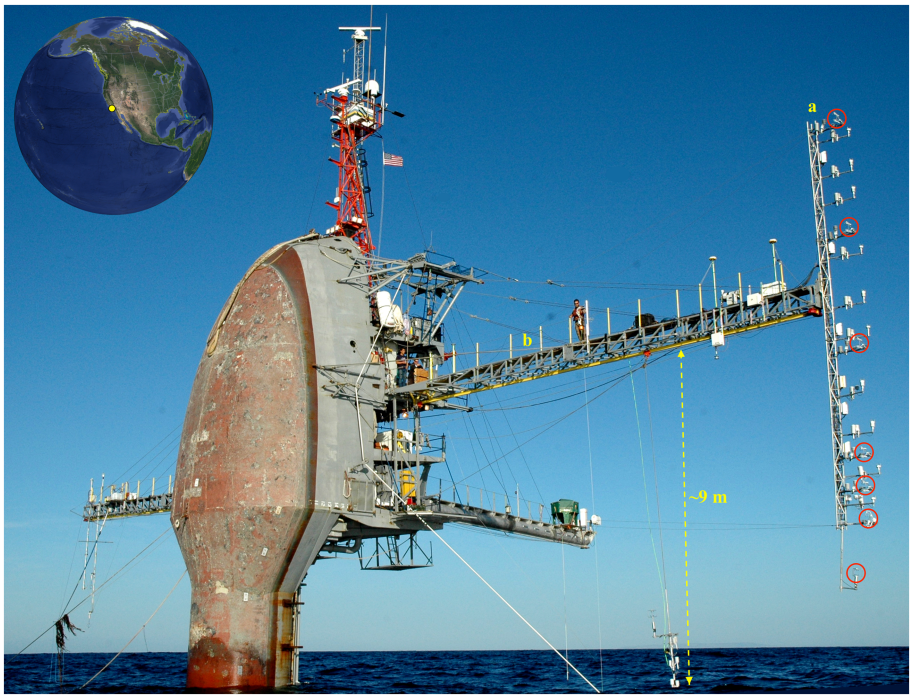

Figure 1. *FLIP* (shown above) is a 108 m long floating platform that stations vertically in the water column and remains very stable under typical oceanic and atmospheric conditions, as compared to a traditional research vessel. Here *FLIP* was moored offshore of Southern California (60 km SW of LAX) and outfitted with a meteorological mast (a) as well as other complimentary observing systems. Here we focus on the data from the seven turbulence-resolving sensors (red circles) on the 13-m-tall mast deployed from *FLIP*'s port boom (b). *FLIP* = Floating Instrument Platform.

variance (energy) spectrum is invariant upon rotation. Condition (1) forms the basis for the concept that small-scale fluid motion is independent of energy-containing scales of the flow, due to the anisotropy of production mechanisms. Condition (2) stems from dimensional arguments that are only valid if ϵ is the only governing parameter (other than k) across the inviscid cascade.

As part of the CASPER project, the Algorithm for Robust Identification of Inertial Subrange (ARIIS) was developed (Ortiz-Suslow, Wang, et al., 2019) to locate Δk in the variance spectrum, by utilizing the isotropy coefficient (Jimenez et al., 1992)

$$I_{ij}(k) = \frac{E_{ii}(k) + k\left(\partial E_{ii}/\partial k\right)}{2E_{jj}}, \tag{2}$$

which converges to unity over an isotropic bandwidth. I_{ij} is the isotropy within the plane defined by the orthogonal components i and j, which may be u, v, or w (the along-, horizontal cross-, and vertical-wind components, respectively). E_{ii}, the observed velocity variance spectrum, is a function of frequency (n) with the transformation to k via Taylor's Frozen Turbulence hypothesis, $k = 2\pi n/U$ (U is the mean wind speed). While debate lingers on the implementation Taylor's hypothesis, we do not expect to lose any generality by substituting Δk for Δn in our analysis. For a given spectrum, the inertial subrange was located by searching from low-to-high n to find the continuous bandwidth where isotropy converged below an investigator-defined threshold. ARIIS uses U/z as the natural low-frequency limit of Δn, and the spectral tails were truncated to avoid entraining high-frequency contaminations into the identified bandwidth. After locating Δn, E_{ii} was statistically analyzed as a log-log function, $\log(E_{ii}) = \mathrm{A} + m_{ii}\log(n)$, where m_{ii} has an expected value of $-5/3$. ARIIS uses an iterative, least squares regression technique to evaluate this expression and derive an empirical estimate for m_{ii}. Samples were eliminated if Δn was insufficiently broad or nonexistent, or the slope across $E_{ii}(n)$ did not converge.

Prior to analysis with ARIIS, the velocity records were filtered using the method described in Hristov et al. (1998) to screen out surface gravity wave signals buried in the turbulence. Also, prior to estimating m_{ii}, the

spectral transfer function (Horst & Oncley, 2006; Pena et al., 2019) was applied to $E_{ii}(n)$ to correct for path averaging. Further details regarding the methods are given in supporting information S2.

3. Results

The velocity variance spectrum can be inspected using wall-layer scaling to facilitate comparison with classical data sets (c.f. Kaimal et al., 1972; Miyake et al., 1970) and highlight the observed turbulence structure. Scaled E_{ii} can take the nondimensional form

$$F_{ii}(f) = \frac{nE_{ii}}{\gamma_i^2} = \alpha_i \phi_\varepsilon^{2/3} f^{m_{ii}}, \tag{3}$$

where α_i and γ_i are the component-wise proportionality and normalization factors, respectively (for $i = u$, $\gamma_i = u_*$, and for $i = v$ *or* w, γ_i is the standard deviation); $\phi_\varepsilon = \left(\kappa z \varepsilon / u_*^3\right)$ is the dimensionless dissipation rate. In (3), the theoretically expected value of $m_{ii} = -2/3$, for all i.

Figure 2 shows F_{ww} from z~16 m above the ocean surface, and the spectra have been segregated by their surface layer stability (ζ), where $\zeta \equiv z/L$ and L is the Obukhov length (Monin & Obukhov, 1954). ζ is related to the Richardson number and is a signed index characterizing the balance between shear and buoyancy turbulence production. In neutral conditions,$|\zeta| \to 0$, turbulence is completely generated by shear production and the MASL is typically in an unstable to near-neutral regime; strongly (un)stable conditions were rare where *FLIP* was stationed.

Figure 2 is comparable to Figures 3 and 4 from Kaimal et al.'s (1972) classical turbulence work over a Kansas wheat field. Across the low frequencies ($f < 1$), our spectra follow a similar ζ-dependent pattern, which reflects the influence of the anisotropic, energy-containing eddies. In Figure 2, we can identify the impact of surface gravity waves on the turbulence structure, particularly for $\zeta > 0$, by the peaks across the gravity wave band, $0.033 < f < 1$. These signals were removed from the spectra prior to running ARIIS, using the Hilbert-Hristov filter. For the high frequencies ($f > 1$), our spectra exhibit the classically observed collapse, but with substantially more spread than those in Kaimal et al., 1972. In particular, there is about a one third of a decade spread across all stabilities, for which stratified conditions exhibit the largest scatter.

3.1. The Observed Variance in m_{ww}

Here we present the findings of our investigation into the variability in m_{ww}, as observed over 23 consecutive days from *FLIP*, representing over 3,800 measurement hours. Though all components were studied, the results for the vertical velocity are the focus here, for conciseness and, more fundamentally, this component may be less influenced by nonstationarity (Hackerott et al., 2017). Herein, the analysis will focus on the spectral slope of the *unscaled* spectrum, $E_{ii}(n)$. The ARIIS-derived slopes were tested against Kolmogorov's expected value, $m_0 = -5/3$ for the unscaled spectra.

Figure 3 summarizes the mean m_{ww} as a function of height above the ocean surface for various subsets of the CASPER-West data (Figure S3, in supporting information, summarizes the aggregate ARIIS results for m_{ww}). We found that the vertical structure, $m_{ww}(z)$, was remarkably consistent across subdata sets representing both typical MASL conditions and cases expected to exhibit Kolmogorovian turbulence. Above 6 m, $m_{ww}(z)$ tended to converge to m_0, but closer to the surface we found a persistent exponential deviation from m_0 toward a flatter slope ($m_{ww} > m_0$). The $m_{ww}(z)$ with the strongest convergence on −5/3, over the largest vertical distance (5–15 m), were cases with exceptionally log-log linear spectra (comprising ~20% of all samples). Profiles exhibiting purely isotropic conditions (I_{uv}~I_{uw}~1) also exhibited very strong convergence on m_0 (< 5% of total data set above 4 m, 11.5% for lowest level) but only above 8 m. The strongest divergence in $m_{ww}(z)$ from m_0, over the entire profile, was for slightly unstable conditions ($-0.2 < \zeta < 0$). In this case, from 4 to 12 m, m_{ww} was consistently 5% larger than m_0—this was the only subset where $m_{ww}(z)$ did not statistically converge on m_0. In summary, while the various $m_{ww}(z)$ are within 10–20% of m_0, indicating Kolmogorov's scaling is approximately valid across much of the MASL, we found significant variance and deviation from m_0 under certain conditions and that there is a distinct and persistent vertical structure in $m_{ww}(z)$.

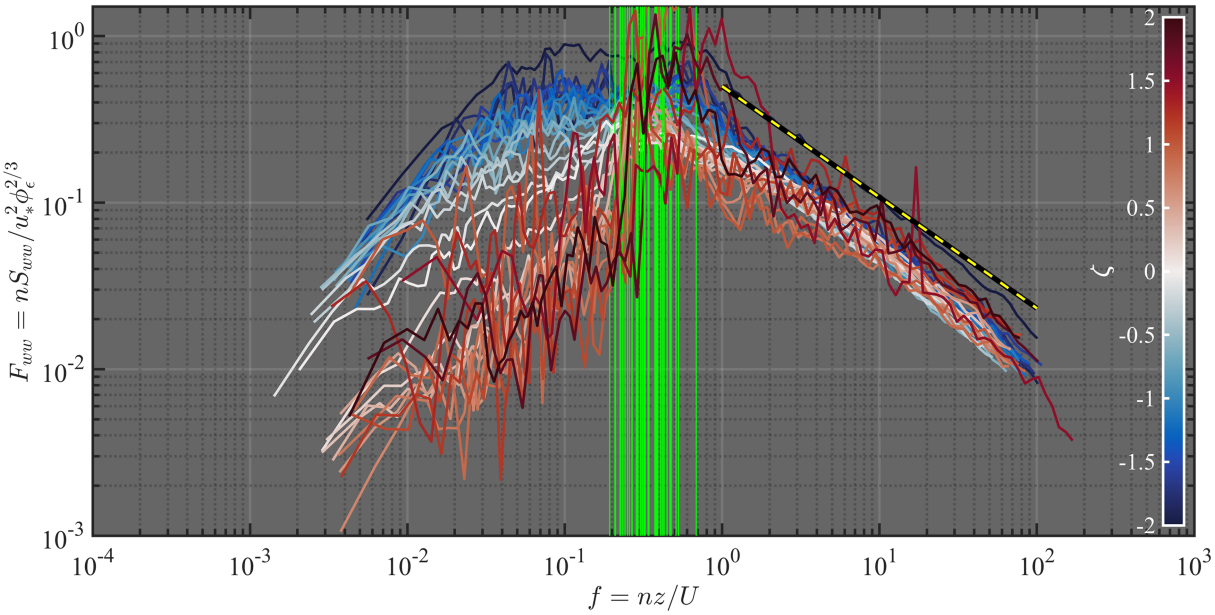

Figure 2. The scaled autovariance spectrum of vertical velocity (F_{ww}) is given as a function of natural frequency ($f = nz/U$) and characterized by ζ, using all of the quality-controlled data analyzed in this study at z= 15.8 m. F_{ww} was scaled following the convention in Kaimal et al., 1972 (which differs from our equation (3) in that $\gamma_w = u_*$). Each individual curve represents the median F_{ww} per increment of 0.1 over the stability range [−2,2]. Warm colors represent stable (stratified) conditions, cool colors depict unstable (convective) conditions. For each representative curve, the corresponding median peak wave frequency is marked as a green vertical line. The dimensionless TKE dissipation rate, ϕ_ε, used to scale S_{ww} was determined from Kaimal et al., 1972 (their equation 7) for consistency. The checkered line exhibits Kolmogorov's slope (−2/3). TKE = turbulence kinetic energy.

3.2. The Dependence of m_{ww} on the Environmental State

The results of our inquiry into $m_{ww}(z)$ suggest that the energy cascade within the MASL could be impacted by the complex air-sea interactions unique to this domain. Variability in MASL dynamics is typically linked to the mean wind speed (U_z) and thermodynamic stability (ζ); and to ascertain the potential mechanisms driving the observed variance in Figure 3, we investigated the dependence of $m_{ww}(z)$ on these parameters (Figure 4). Given the results in Figure 3, we also examined the variability of $m_{ww}(z)$ as a function of the surface gravity waves, which we characterized here by the relationship between the dominant wave phase speed C and the turbulent friction velocity u_*, defined as the wave age C/u_*. These results are shown in Figure 5.

For all levels, m_{ww} did exhibit a relationship with U_z (Figure 4i), with a clear distinction in the nature of this dependence between the two levels closest to the surface and the upper profile (5–16 m). For the latter, m_{ww} was well described as a linear function ($m_{ww} = aU_z+B$) over the range $3 < U_z < 15$, with the slope (intercept) tending to decrease (increase) with z. The methodology and results of this linear regression are presented in supporting information S4 and Table S4. There is lingering uncertainty regarding the behavior of m_{ww} at very low winds, due to the collapsing signal-to-noise in the sonic anemometry; therefore, these data were not considered in the regression analysis. As a purely empirical exercise, extrapolating the z dependence of a, we found that $a \to 0$ at ~27 m. Independently, we determined the height at which $B \to m_0$ to be ~50 m. While separately the a and B coefficients were strong linear functions of z, the significance of this extrapolation is limited, but it may indicate that a substantial fraction of the total MASL *could* exhibit the $m_{ww}(U_z)$ we observed. The linear coefficients (with 95% confidence bounds), estimated from the aggregated upper profile data set, were $a = 0.0112 \pm 0.21$ and $B = -1.714 \pm 0.039$ ($r^2 = 0.19$, p value $p < 0.001$).

For the lowest two levels, the variation of m_{ww} with U_z was evident but significantly different from the higher levels. Below U_z~ 6 m/s, both levels exhibited a rapid increase in m_{ww}, 2–3 times larger than the upper levels; and for these two lowest levels, $m_{ww}(U_z)$ was weakly linear ($r^2 \sim 0.1$). Above 6 m/s, m_{ww} in the lowest level

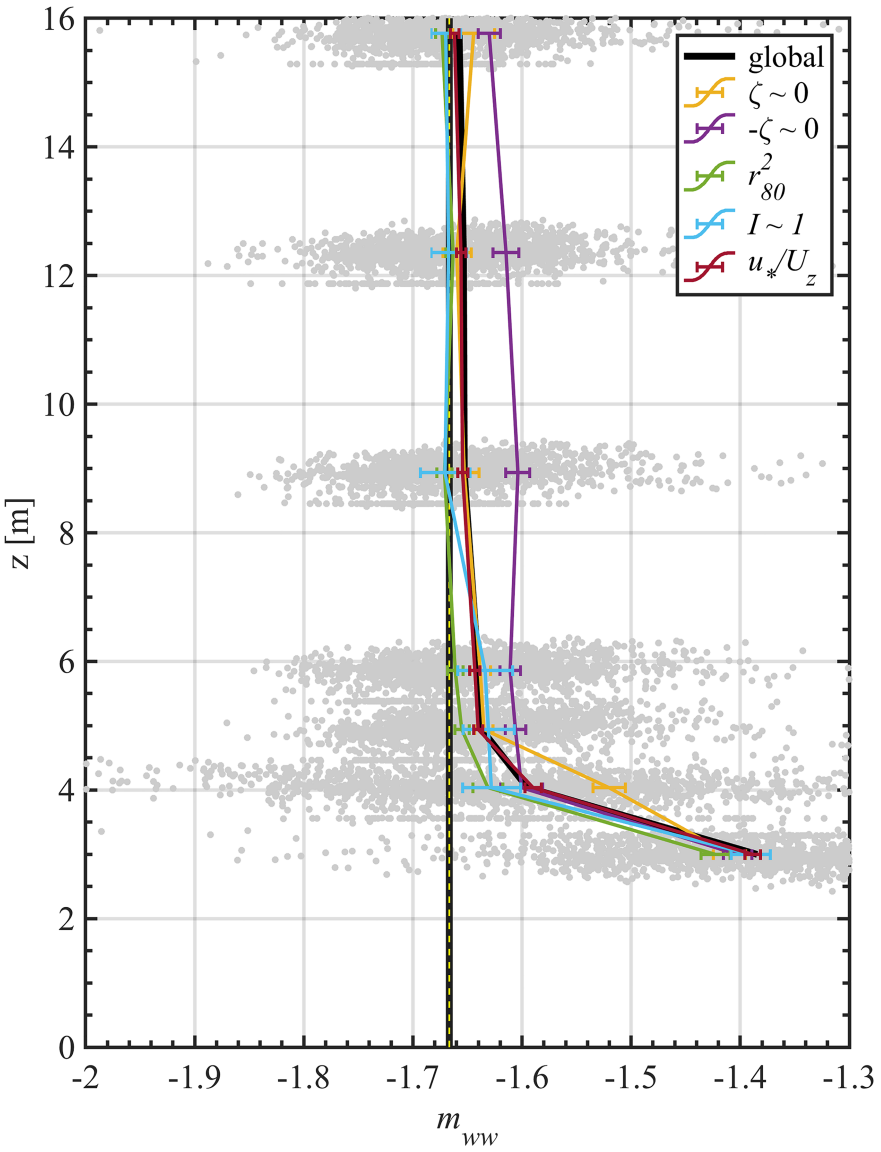

Figure 3. The total observation cloud (gray dots) for each z underneath mean profiles of m_{ww} for different subsets of the complete data set (error bars span ±2× the standard error of the mean). The black-gold checkered line marks m_0. The different curves represent sets of m_{ww}: all observations (black), slightly stable (orange), slightly unstable (purple), 80th percentile of r^2 (i.e., the most log-log linear spectra; green), near isotropic conditions (light blue), and turbulence intensity index (maroon). Near-neutral conditions (ζ~0 and $-\zeta$~0) were represented as $0 \leq |\zeta| \leq 0.2$; purely isotropic conditions were defined as when both u-w and u-v plane I $\in$[0.9,1.1]; for u_*/U_z, the curve represents typical conditions [0.02,0.05].

appears to level off, with the penultimate level abruptly transitioning to being in line with the trends of the upper profile, but with persistently higher intersample variance. The complex, nonlinear response of these lowest levels suggests multiple regime transitions in the inertial energy cascade near the interface as MASL wind forcing increases.

Our investigation into the dependence of $m_{ww}(\zeta)$ yielded mixed results (Figures 4ii and 4iii). Closest to the surface, we found a negative dependence on$|\zeta|$. At the penultimate level, m_{ww} (ζ) was consistent with the upper profile for all ζ except in the case of $\zeta \to 1$. All upper levels behaved consistently, with a slight positive trend as $-\zeta \to 0$ and no clear dependence when $\zeta > 0$. For the lowest three levels across the upper profile (5–8 m), a slight positive trend was evident in $m_{ww}(\zeta)$, as stability increases to stable-strongly stable, but there are two few observations within this regime to confirm this behavior.

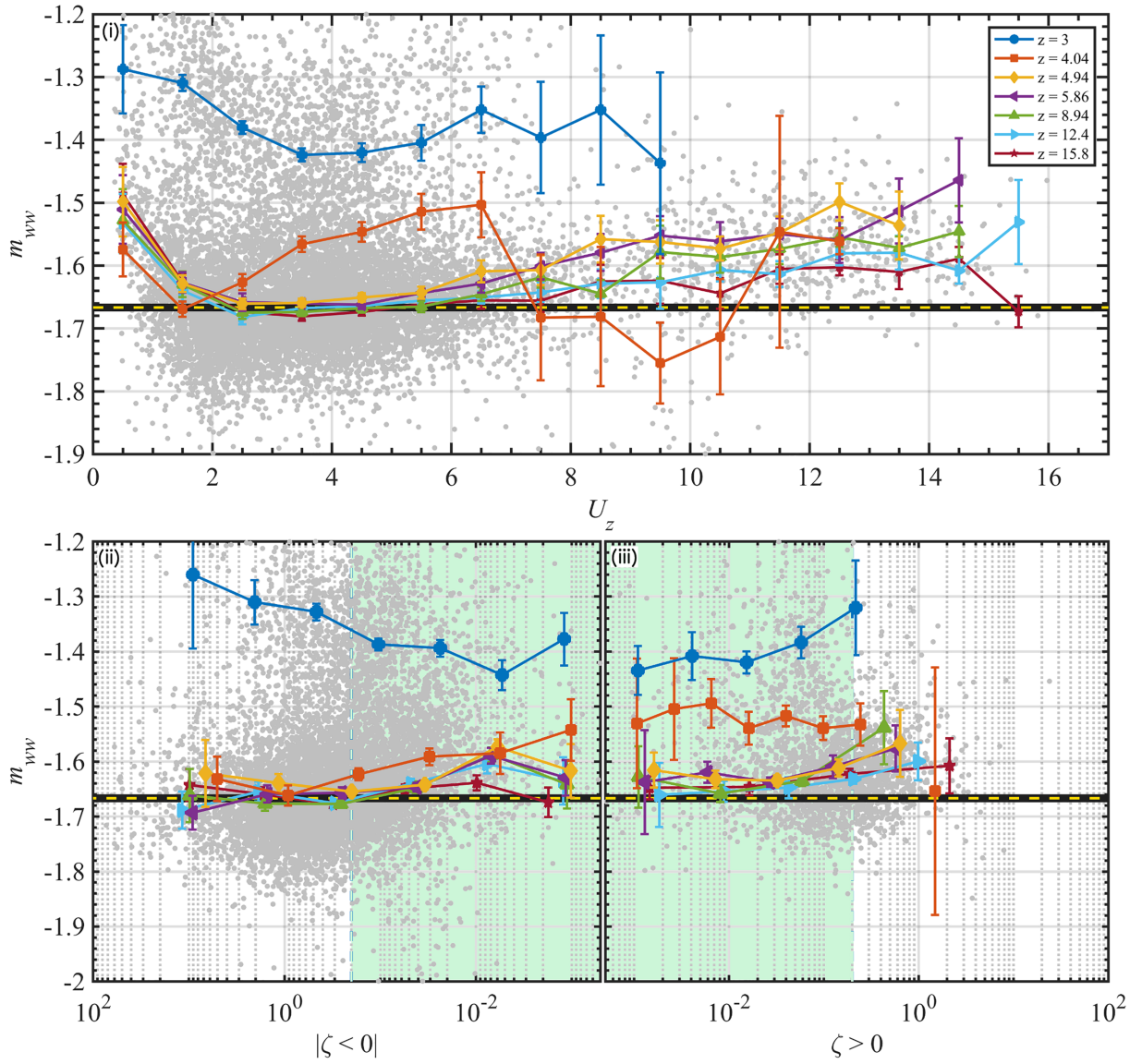

Figure 4. (i) m_{ww} given as a function of the mean wind speed (U_z) at each level z above the surface. The total observation cloud (gray) is given underneath bin-averaged (1-m/s discrete steps) curves. (ii and iii) Analysis of m_{ww} dependence on ζ. Bin averaging was limited to |0.001,100| and used a log-uniform bin width. The black-gold checkered line marks m_0 in all panels; all error bars span ±2x the standard error.

Wave age (C/u_*) characterizes the relative motion between the waves and wind; it is a key parameter used for describing the wave field development and the energy flux from the tangential wind stress into the surface waves. For the upper levels, $m_{ww} \rightarrow m_0$ for $5 < C/u_* < 20$, which represents the mean wave age condition, but for the extrema conditions (very young and old, respectively) we found m_{ww} tending to diverge from m_0 for all z. Again, the penultimate level exhibits mixed behavior, with regimes conforming to the lowest level ($C/u_* < 5$) and the upper profile ($C/u_* \rightarrow \infty$), respectively. The lowest level exhibited a strong positive relationship with C/u_* in the transition to swell-dominated conditions—the incongruous drop in $m_{ww}(z = 3)$ at C/u_*~70 may be attributed to too few samples at this limit.

4. Discussion

Kolmogorov's power law is expected to vary slightly due to intermittency (Oboukhov, 1962), but the extent of this deviation has been elusive to quantify using experimental, much less geophysical data. Barenblatt and Chorin argued that for large but finite *Re*, the impact of intermittency becomes negligible (Barenblatt &

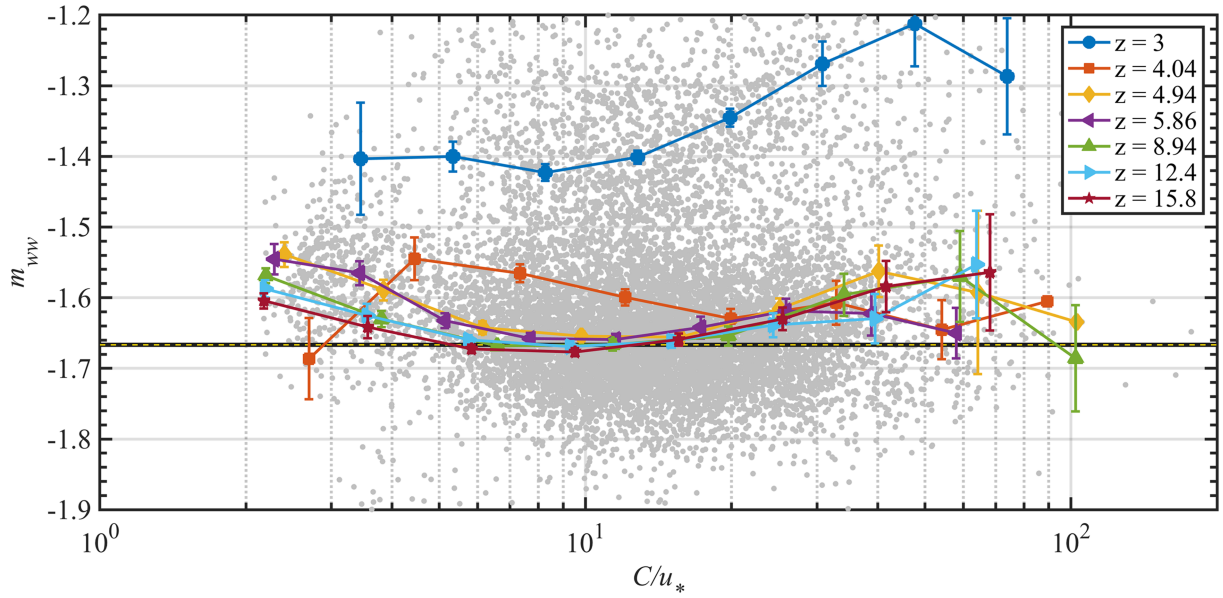

Figure 5. m_{ww} given as a function of wave age, C/u_*, using the phase speed (C) of the dominant waves, for each measurement level. The total observation cloud was filtered using a logarithmically uniform bin average over the range [1,200]; error bars span 2 times the standard error.

Chorin, 1997). For our entire data set, a crude estimation of Re is ~10^8 and, regardless, intermittency exerts significantly more influence during stable conditions, as observed over land (Vindel & Yagüe, 2011). In our data, we observed no clear dependence of m_{ww} on $\zeta > 0$, though we do not capture sufficient data in strongly stable conditions. Given the high Re and generally unstratified conditions reflected in these data, it is unlikely that intermittency primarily explains the deviation from the m_0 slope reported here.

Our results indicate persistent deviations from m_0 that depended on the height above the ocean surface and various mean parameters reflective of the dynamics within the air-sea interfacial domain. In our preanalysis work, we have made a particular effort to either correct or remove samples significantly impacted by experimental biases or noise and it seems implausible that, in general, methodological factors could reasonably explain the divergence from m_0 we observed. Figures 4i and 5 do indicate that the slope dramatically increases as the wind speed goes to zero, which makes interpretation of the physicality of this response difficult due to the signal-to-noise approaching unity. However, this should only be the case for $U_z < 2$ m/s. Outside of this regime, we hypothesize that the distinct and persistent trends in the empirically derived inertial subrange slope may be attributable to the presence of surface gravity waves and the subsequent wind-wave-turbulence interactions that are unique to this wall-bounded shear flow. While non-Kolmogorovian turbulence is expected under certain flow regimes (even at large Re), this has never been theoretically or experimentally characterized near a wavy surface.

Recent experimental work has established that, near the surface, localized wind shear varies coherently with the surface deflection driven by the wave motion at the interface (Buckley & Veron, 2016; Grare et al., 2013). When phase-averaged, this generates a nonproductive stress component (Janssen, 1989), which dominates within the atmospheric wave boundary layer. This wave-coherent stress can be removed from the turbulent velocity record (following Hristov et al., 1998), but a comparison of our prefiltered and postfiltered ARIIS output revealed an aggregate <1% change in the estimated m_{ww}. We posit that, instantaneously, these wave-coherent wind gradients generate turbulent stresses, through localized wind shear, which is likely independent from the macroscopic airflow. This would provide a mechanism for air-wave-turbulence interaction that could inject inertial energy into the cascade already developed by the mean kinetic motion of the wind. Critically, this energy would not be removed by the Hilbert-Hristov filter because it occurs at frequencies above the gravity wave band.

We have initiated a separate analysis on the vertical stress divergence observed from *FLIP,* which may provide tangential support for this hypothesis. After removing cases with strong vertical variation of u_*, the mean m_{ww} across all levels was found to shift substantially toward −5/3 and the overall variance was

reduced by 30–50%. The largest shifts in m_{ww} occurred nearest to the surface, implying that the noninertial stresses may have contributed to the observed deviation from −5/3. However, these are preliminary findings. While the implications are intriguing, further in-depth analysis is part of the future work that goes beyond the scope of the present study.

5. Conclusions

We have presented the first systematic, observation-based evaluation of Kolmogorov's inertial subrange power law within the MASL. Our investigation yielded two primary results: (1) the observed spectral scaling across the inertial subrange across much of the MASL was within 10–20% of the theoretical value, but that (2) buried within this variance was systematic dependence on the mean environmental state and air-sea dynamical regime. The variance and mean divergence from −5/3 in the observed scaling (m_{ww}) increased substantially with proximity to the wavy surface. Our results provide evidence for a hitherto unaccounted role played by surface gravity waves in controlling the structure of fine-scale turbulent motions near the air-sea interface. While we were able to link the observed spectral slope to typically available MASL parameters, this analysis does not fundamentally address the underlying mechanisms driving this non-Kolmogorovian turbulence. Additional study is needed to fully explore these mechanisms and develop a new physical framework that can be incorporated into the study of turbulence dynamics on both sides of the interface. As a final note, we also found that purely isotropic conditions are exceptionally rare in the MASL (see Figure S3). While pure isotropic conditions are not necessarily expected in the real atmosphere, especially near a surface (Wyngaard, 2010), the degree of the anisotropy we observed had not been previously documented. The implications this has on both our theoretical and practical knowledge of atmospheric turbulence should be the focus of continued investigations.

Acknowledgments
This work would not have been possible without their efforts in data collection and processing by Ryan Yamaguchi and John Kalogiros. Also, other NPS Boundary Layer Processes group members, Denny Alappattu, Richard Lind, Alex Olson, Ben Wauer, Kyle Franklin, and Anna Hook, were instrumental in the data collection phase of this work. The authors would like to especially acknowledge the Captain and crew of the *FLIP* for their tireless efforts during the cruise and without whom we would not have such unique data set. The authors thank A. Arenas for his comments and feedback as part of the background research on this topic. The data used in this study are publicly available through an open access repository: https://nps.box.com/shared/static/di5887nl4g3thgz6bz67z3l44tj77qur.zip. The updated source code for ARIIS can be accessed from www.github.com/dortizsu/ARIIS. Q. W. conceived of and designed the experiments. D. O.-S. and Q. W. conducted the measurements. D. O.-S. carried out the detailed data processing and analysis. D. O.-S. and Q. W. interpreted the findings and wrote the manuscript. The authors declare no competing interests. This work was supported through the Coupled Air-Sea Processes and Electromagnetic ducting Research (CASPER) project funded by the U.S. Office of Naval Research grant N0001419WX01369 under its Multidisciplinary University Research Initiative (MURI). Q. W. is also supported by the Quantifying and Understanding Environmental Turbulence Affecting Lasers (QueTal) project funded by the Directed Energy Joint Technology Office (DEJTO) grant (F2KBAB8159G002).

References

Abraham, E. R. (1998). The generation of plankton patchiness by turbulent stirring. *Nature*, *391*(6667), 577–580. https://doi.org/10.1038/35361

Anderson, R. J. (1993). A study of wind stress and heat flux over the open ocean by the inertial-dissipation method. *Journal of Physical Oceanography*, *23*(10), 2153–2161. https://doi.org/10.1175/1520-0485(1993)023<2153:ASOWSA>2.0.CO;2

Arenas, A., & Chorin, A. J. (2006). On the existence and scaling of structure functions in turbulence according to the data. *Proceedings of the National Academy of Sciences of the United States of America*, *103*(12), 4352–4355. https://doi.org/10.1073/pnas.0600482103

Barenblatt, G. I., & Chorin, A. J. (1997). Scaling laws and vanishing-viscosity limits for wall-bounded shear flows and for local structure in developed turbulence. *Communications on Pure and Applied Mathematics*, *50*(4), 381–398. https://doi.org/10.1002/(SICI)1097-0312(199704)50:4<381::AID-CPA5>3.0.CO;2-6

Barenblatt, G. I., Chorin, A. J., & Prostokishin, V. M. (1997). Scaling laws for fully developed turbulent flow in pipes*. *Applied Mechanics Reviews*, *50*(7), 413–430. Retrieved from. https://math.berkeley.edu/~chorin/BCP97.pdf

Barenghi, C. F., Sergeev, Y. A., & Baggaley, A. W. (2016). Regimes of turbulence without an energy cascade. *Scientific Reports*, *6*(1), 1–11. https://doi.org/10.1038/srep35701

Batchelor, G. K. (1947). Kolmogoroff's theory of locally isotropic turbulence. *Mathematical Proceedings of the Cambridge Philosophical Society*, *43*(04), 533. https://doi.org/10.1017/S0305004100023793

Batchelor, G. K. (1953). The universal equilibrium theory. In *The theory of homogeneous turbulence* (pp. 103–132). New York, New York: Cambridge University Press.

Buckley, M. P., & Veron, F. (2016). Structure of the airflow above surface waves. *Journal of Physical Oceanography*, *46*(5), 1377–1397. https://doi.org/10.1175/JPO-D-15-0135.1

Drennan, W. M., Kahma, K. K., & Donelan, M. A. (1999). On momentum flux and velocity spectra over waves. *Boundary-Layer Meteorology*, *92*(3), 489–515. https://doi.org/10.1023/A:1002054820455

Dreyer, G. F. (1974). Comparison of momentum, sensible and latent heat fluxes over the open ocean determined by the direct covariance, inertial and direct dissipation techniques. University of California, San Diego.

Durand, P., De Sa, L., Druilhet, A., & Said, F. (1991). Use of the inertial dissipation method for calculating turbulent fluxes from low-level airborne measurements. *Journal of Atmospheric and Oceanic Technology*, *8*(1), 78–84. https://doi.org/10.1175/1520-0426(1991)008<0078:UOTIDM>2.0.CO;2

Edson, J. B., & Fairall, C. W. (1998). Similarity relationships in the marine atmospheric surface layer for terms in the TKE and scalar variance budgets. *Journal of the Atmospheric Sciences*, *55*(13), 2311–2328. https://doi.org/10.1175/1520-0469(1998)055<2311:SRITMA>2.0.CO;2

Edson, J. B., Fairall, C. W., Mestayer, P. G., & Larsen, S. E. (1991). A study of the inertial-dissipation method for computing air-sea fluxes. *Journal of Geophysical Research*, *96*(C6), 23. https://doi.org/10.1029/91jc00886

Fairall, C. W., & Larsen, S. E. (1986). Inertial-dissipation methods and turbulent fluxes at the air-ocean interface. *Boundary-Layer Meteorology*, *34*(3), 287–301. https://doi.org/10.1007/BF00122383

Fisher, F. H., & Spiess, F. N. (1963). FLIP-Floating Instrument Platform. *The Journal of the Acoustical Society of America*, *35*(10), 1633–1644. https://doi.org/10.1121/1.1918772

Friehe, C. A., La Rue, J. C., Champagne, F. H., Gibson, C. H., & Dreyer, G. F. (1975). Effects of temperature and humidity fluctuations on the optical refractive index in the marine boundary layer. *Journal of the Optical Society of America*, *65*(12), 1502–1511.

Grachev, A. A., Leo, L. S., Fernando, H. J. S., Fairall, C. W., Creegan, E., Blomquist, B. W., et al. (2018). Air-sea/land interaction in the coastal zone. *Boundary-Layer Meteorology*, *167*(2), 181–210. https://doi.org/10.1007/s10546-017-0326-2

Grare, L., Lenain, L., & Melville, W. K. (2013). Wave-coherent airflow and critical layers over ocean waves. *Journal of Physical Oceanography*, *43*(10), 2156–2172. https://doi.org/10.1175/JPO-D-13-056.1

Hackerott, J. A., Bakhoday-Paskyabi, M., Reuder, J., de Oliveira, A. P., Kral, S. T., Marques Filho, E. P., et al. (2017). A surface-layer study of the transport and dissipation of turbulent kinetic energy and the variances of temperature, humidity and CO_2. *Boundary-Layer Meteorology*, *165*(2), 211–231. https://doi.org/10.1007/s10546-017-0271-0

Hogstrom, U. (1996). Review of some basic characteristics of the atmospheric surface layer*. *Boundary-Layer Meteorology*, *78*(3–4), 215–246 . Retrieved from. https://link.springer.com/content/pdf/10.1007/BF00120937.pdf

Horst, T. W., & Oncley, S. P. (2006). Corrections to inertial-range power spectra measured by CSAT3 and solent sonic anemometers, 1. Path-averaging errors. *Boundary-Layer Meteorology*, *119*(2), 375–395. https://doi.org/10.1007/s10546-005-9015-7

Hristov, T., Friehe, C., & Miller, S. (1998). Wave-coherent fields in air flow over ocean waves: Identification of cooperative behavior buried in turbulence. *Physical Review Letters*, *81*(23), 5245–5248. https://doi.org/10.1103/PhysRevLett.81.5245

Janssen, P. A. E. M. (1989). Wave-induced stress and the drag of air flow over sea waves. *Journal of Physical Oceanography*, *19*(6), 745–754. https://doi.org/10.1175/1520-0485(1989)019<0745:WISATD>2.0.CO;2

Jimenez, J., Wray, A. A., Saffman, P. G., & Rogallo, R. S. (1992). The structure of intense vorticity in homogeneous isotropic turbulence. *Center for Turbulence Research: Proceedings of the Summer Program*, 24. Retrieved from https://ntrs.nasa.gov/search.jsp? R = 19940010274

Kaimal, J. C., Wyngaard, J. C., Izumi, Y., & Cote, O. R. (1972). Spectral characteristics of surface-layer turbulence. *Quarterly Journal of the Royal Meteorological Society*, *98*(417), 563–589. https://doi.org/10.1002/qj.49709841707

Kolmogorov, A. N. (1941a). Dissipation of energy in locally isotropic turbulence. *Comptes Rendus de l'Acadamie Des Sciences de l'U.R.S.S*, *32*(16).

Kolmogorov, A. N. (1941b). The local structure of turbulence in incompressible viscous fluid for very large Reynolds numbers. *Doklady Akademii Nauk SSSR* Retrieved from. http://homepages.see.leeds.ac.uk/~eeaol/p/kolmogorov41.pdf

Kolmogorov, A. N. (1962). A refinement of previous hypotheses concerning the local structure of turbulence in a viscous incompressible fluid at high Reynolds number. *Journal of Fluid Mechanics*, *13*(01), 82. https://doi.org/10.1017/S0022112062000518

Large, W. G., & Pond, S. (1981). Open ocean momentum flux measurements in moderate to strong winds. *Journal of Physical Oceanography*, *11*, 13.

Large, W. G., & Pond, S. (1982). Sensible and latent heat flux measurements over the ocean. *Journal of Physical Oceanography*, *12*(5), 464–482. https://doi.org/10.1175/1520-0485(1982)012<0464:SALHFM>2.0.CO;2

Lawrence, R. S., Ochs, G. R., & Clifford, S. F. (1970). Measurements of atmospheric turbulence relevant to optical propagation. *Journal of the Optical Society of America*, *60*(6), 826. https://doi.org/10.1364/JOSA.60.000826

MacCready, P. (1962). The inertial subrange of atmospheric turbulence. *Journal of Geophysical Research*, *67*(3), 1051–1059.

Martínez-Prat, B., Ignés-Mullol, J., Casademunt, J., & Sagués, F. (2019). Selection mechanism at the onset of active turbulence. *Nature Physics*, *15*(4), 362–366. https://doi.org/10.1038/s41567-018-0411-6

Miller, S. D., Hristov, T. S., Edson, J. B., & Friehe, C. A. (2008). Platform motion effects on measurements of turbulence and air–sea exchange over the open ocean. *Journal of Atmospheric and Oceanic Technology*, *25*, 1683–1694. https://doi.org/10.1175/2008JTECHO547.1

Miyake, M., Stewart, R. W., & Burling, R. W. (1970). Spectra and cospectra of turbulence over water. *Quarterly Journal of the Royal Meteorological Society*, *96*(407), 138–143. https://doi.org/10.1002/qj.49709640714

Moffatt, H. K. (2002). G.K. Batchelor and the homogenization of turbulence. *Annual Review of Fluid Mechanics*, *34*, 19–35. Retrieved from. www.annualreviews.org

Monin, A. S., & Obukhov, A. M. (1954). Basic laws of turbulent mixing in the surface layer of the atmosphere. *Trudy Akademiia Nauk SSSR Geophiz*, *24*(151), 30.

Muñoz-Esparza, D., Sharman, R. D., & Lundquist, J. K. (2018). Turbulence dissipation rate in the atmospheric boundary layer: Observations and WRF mesoscale modeling during the XPIA field campaign. *Monthly Weather Review*, *146*(1), 351–371. https://doi.org/10.1175/MWR-D-17-0186.1

Oboukhov, A. M. (1962). Some specific features of atmospheric tubulence. *Journal of Fluid Mechanics*, *13*(01), 77. https://doi.org/10.1017/S0022112062000506

Ortiz-Suslow, D. G., Wang, Q., Kalogiros, J. A., & Yamaguchi, R. (2019). A method for identifying Kolmogorov's inertial subrange in the velocity variance spectrum. *Journal of Atmospheric and Oceanic Technology*. https://doi.org/10.1175/JTECH-D-19-0028.1

Ortiz-Suslow, D. G., Kalogiros, J., Yamaguchi, R., Alappattu, D., Franklin, K., Wauer, B., & Wang, Q. (2019). *The data processing and quality control of the marine atmospheric boundary layer measurement systems deployed by the Naval Postgraduate School during the CASPER-West field campaign*. Monterey, CA: Calhoun. https://doi.org/NPS-MR-19-001

Payne, F. R., & Lumley, J. L. (1966). One-dimensional spectra derived from an airborne hot-wire anemometer. *Quarterly Journal of the Royal Meteorological Society*, *92*(393), 397–401. https://doi.org/10.1002/qj.49709239309

Peinke, J., Barth, S., Böttcher, F., Heinemann, D., & Lange, B. (2004). Turbulence, a challenging problem for wind energy. *Physica A: Statistical Mechanics and its Applications*, *338*(1–2), 187–193. https://doi.org/10.1016/J.PHYSA.2004.02.040

Pena, A., Ebba, D., & Mann, J. (2019). A method to assess the accuracy of sonic anemometer measurements. *Atmospheric Measurement Techniques*, *12*, 237–252. https://doi.org/10.5194/amt-12-237-2019

Phelps, G. T., & Pond, S. (1971). Spectra of the temperature and humidity fluctuations and of the fluxes of moisture and sensible heat in the marine boundary layer. *Journal of the Atmospheric Sciences*, *28*(6), 918–928. https://doi.org/10.1175/1520-0469(1971)028<0918:SOTTAH>2.0.CO;2

Sjöblom, A., & Smedman, A. (2002). The turbulent kinetic energy budget in the marine atmospheric surface layer. *Journal of Geophysical Research*, *107*(C10), 3142. https://doi.org/10.1029/2001JC001016

Tennekes, H., & Lumley, J. L. (1972). *A first course intturbulence*. Cambridge, Massachusetts: MIT Press.

Vindel, J. M., & Yagüe, C. (2011). Intermittency of Turbulence in the atmospheric boundary layer: Scaling exponents and stratification influence. *Boundary-Layer Meteorology*, *140*(1), 73–85. https://doi.org/10.1007/s10546-011-9597-1

Wang, Q., Alappattu, D. P., Billingsley, S., Blomquist, B., Burkholder, R. J., Christman, A. J., et al. (2018). CASPER: Coupled air-sea processes and electromagnetic (EM) ducting research. *Bulletin of the American Meteorological Society*, *99*(7), 1449–1471. https://doi.org/10.1175/BAMS-D-16-0046.1

Wensink, H. H., Dunkel, J., Heidenreich, S., Drescher, K., Goldstein, R. E., Löwen, H., & Yeomans, J. M. (2012). Meso-scale turbulence in living fluids. *Proceedings of the National Academy of Sciences of the United States of America*, *109*(36), 14308–14313. https://doi.org/10.1073/pnas.1202032109

Wyngaard, J. C. (2010). *Turbulence in the atmosphere*, (1st ed.). Cambridge: Cambridge University Press.

Yaglom, M. A. (1981). Laws of small scale turbulence in atmosphere and ocean (in commemoration of the 40th anniversary of the theory of locally isotropic turbulence). *Izvestiya Atmospheric and Oceanic Physics*, *17*, 1235–1257. Retrieved from. https://ci.nii.ac.jp/naid/80014277021/

Yelland, M., & Taylor, P. K. (1996). Wind stress measurements from the open ocean. *Journal of Physical Oceanography*, *26*, 18.

Yeung, P. K., & Zhou, Y. (1997). Universality of the Kolmogorov constant in numerical simulations of turbulence. *Physical Review E*, *56*(2), 1746. Retrieved from https://journals.aps.org/pre/pdf/10.1103/PhysRevE.56.1746